Communication
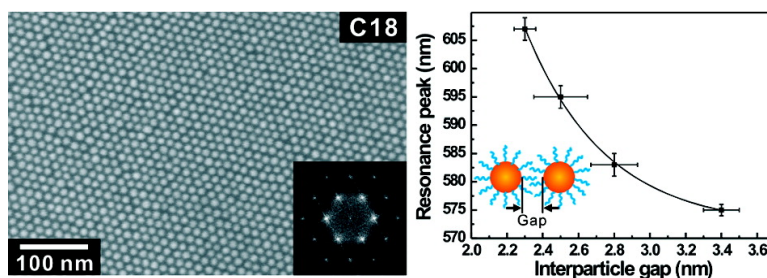
Tunable Plasmonic Response from Alkanethiolate-Stabilized Gold Nanoparticle Superlattices: Evidence of Near-Field Coupling

Chi-Fan Chen, Shien-Der Tzeng, Hung-Ying Chen, Kuan-Jiuh Lin, and Shangjr Gwo

More About This Article

Additional resources and features associated with this article are available within the HTML version:

- Supporting Information
- Links to the 6 articles that cite this article, as of the time of this article download
- Access to high resolution figures
- Links to articles and content related to this article
- Copyright permission to reproduce figures and/or text from this article

View the Full Text HTML

Tunable Plasmonic Response from Alkanethiolate-Stabilized Gold Nanoparticle Superlattices: Evidence of Near-Field Coupling

Chi-Fan Chen,[†] Shien-Der Tzeng,[‡] Hung-Ying Chen,[†] Kuan-Jiuh Lin,[‡] and Shangjr Gwo*,[†]

Institute of Nanoengineering and Microsystems and Department of Physics, National Tsing-Hua University, Hsinchu 30013, Taiwan, Republic of China, and Department of Chemistry and Center for Nanoscience and Nanoengineering, National Chung-Hsing University, Taichung 402, Taiwan, Republic of China

Received September 23, 2007; E-mail: gwo@phys.nthu.edu.tw

Noble metal nanoparticles exhibit a strong optical resonance phenomenon that is absent in the bulk phase. The related extinction band has been understood to be caused by a collective oscillation of conduction electrons in the nanoparticles under optical excitation and is characterized as the localized surface plasmon resonance (LSPR) band.[1] Previous studies show that the LSPR band is sensitive to nanoparticle composition, size, shape, local dielectric environment, and electromagnetic coupling to other proximate nanoparticles.[1−4] Recently, considerable attention has been given to the studies of coupled nanoparticle pairs[5] as well as one-dimensional (1D)[6] and two-dimensional (2D)[7] nanoparticle arrays prepared by electron-beam lithography (EBL) because of their interesting and potentially useful collective plasmonic properties, which can be important in the emerging fields of plasmonics-based subwavelength optics.[8] In principle, two types of electromagnetic interaction can be exploited for controlling collective surface plasmon resonance (CSPR) of nanoparticle arrays, including near-field coupling and far-field dipole−dipole interaction.[9] Near-field coupling is especially relevant for nearly touching, ultrasmall colloidal nanoparticles due to the short spatial range of the evanescent near fields. In addition to the size advantage, colloidal nanoparticles possess superior plasmonic properties,[10] and their near-field coupling can lead to coherent (in-phase) interactions between adjacent colloidal nanoparticles. In such a way, arrays of colloidal nanoparticles can act as "plasmonic crystals" with coherent plasmonic response and minimized losses.

Here we report on the self-assembly of large-area, highly ordered 2D superlattices of alkanethiolate-stabilized gold nanoparticles onto quartz substrates with varying lattice constants, which can be controlled by the alkyl chain lengths, ranging from C12 (1-dodecanethiolate), C14 (1-tetradecanethiolate), C16 (1-hexadecanethiolate), to C18 (1-octadecanethiolate). These 2D nanoparticle superlattices show strong CSPR extinction bands which are tunable via near-field coupling of adjacent nanoparticles. In this work, pronounced chain-length-dependent red shifts have been confirmed for synthesized superlattices. Furthermore, evidence of near-field coupling such as the exponential dependent red shift with decreasing interparticle separation gap (edge-to-edge) is clearly demonstrated. The approach presented here allows for an unprecedented lattice control of artificial plasmonic crystals with the tunability precision of interparticle gap on an atomic scale.

In the conventional one-step, two-phase Brust−Schiffrin method[11a] for the synthesis of gold nanoparticles with a protection monolayer of alkanethiolates, the tetrachloroaurate ions ($AuCl_4^-$) in the aqueous solution are transferred to the organic solution (toluene) using a phase transfer agent and reduced in the presence of reducing agent and thiol. However, methods of forming gold nanoparticles

in the presence of alkanethiols can only be used to synthesize small (<5 nm in diameter)[12] particles, which are not optimized for applications in plasmonics due to large damping coefficients (inversely proportional to the particle size due to enhanced surface scattering of the conduction electrons). Moreover, it was found that, as the thiolate chain length increases, the synthesized nanoparticles become more polydispersed (with a broader size distribution) and larger in mean size.[12c] Therefore, we have adopted for this work a two-step, two-phase method for synthesizing thiolate-protected gold nanoparticles.[11b] In short, large-size [∼10.5 nm in diameter (d), Figure S1] and monodispersed (∼5.8%, Figure S2 and Table S1) gold nanoparticles were first synthesized by the aqueous Turkevich method, in which $AuCl_4^-$ was reduced by trisodium citrate. In the second step, the aqueous gold nanoparticles were transferred to toluene and capped with alkanethiolates of different chain lengths using a modified two-phase method (see details in Supporting Information). In this approach, larger-sized gold nanoparticles of the same mean diameter and size distribution can be synthesized with different thiolate capping (Au@C12, Au@C14, Au@C16, and Au@C18).

Natural dewetting process (e.g., by slow evaporation of nanoparticle-containing solvent on a support) was typically applied for forming hexagonal close-packed (HCP) 2D nanoparticle superlattices.[12] However, the nanoparticle superlattices formed by this approach are typically quite irregular in ordering (polycrystalline) and have a small spatial extent, usually less than 1 μm. Lin et al. succeeded in forming large-area (over several microns) gold nanoparticle superlattices (∼5.5 nm in diameter) onto silicon nitride films by using kinetic control of the dewetting process with increasing concentration of the nonvolatile dodecanethiol ligand.[12d] In this work, due to the aforementioned consideration regarding the nanoparticle size limitation, we adopted a different approach for nanoparticle synthesis and surface functionalization. Moreover, by controlling the dewetting temperature of the solvent, long-range-ordered nanoparticle superlattices can be prepared routinely (see Supporting Information for details), with the single domain size extending over 1 mm² for the case of Au@C18 nanoparticle superlattices (Figure 1). The long-range ordering of superlattices is also evidenced by diffraction patterns shown in Figure 2b. The excellent agreement between real-space (Figure 2a) and reciprocal-space (Figure 2b) lattice analysis over wide regions of nanoparticle superlattices demonstrates the high "crystalline" quality of self-assembled nanoparticle superlattices. Using the lattice constants (a) shown in Figure 2a, the interparticle gap length l ($= a - d$) of the HCP nanoparticle arrays has been found to be linearly dependent on the length (nm) of the alkyl chains ($l = 0.83 + 0.122n$, where n is the number of carbon atoms per chain) for the cases of Au@C12, Au@C14, and Au@C16 superlattices. Also, the interparticle gap was found to be about 60% of the expected value for


[†] National Tsing-Hua University.
[‡] National Chung-Hsing University.
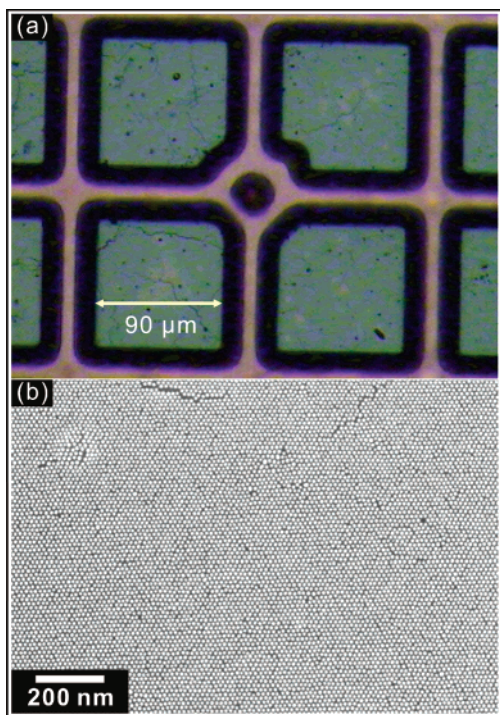
Figure 1. (a) Optical microscope image of hexagonal close-packed (HCP) 2D superlattice self-assembled by octadecanethiolate-stabilized gold nanoparticles (Au@C18) onto a quartz substrate. The self-assembled Au@C18 nanoparticle superlattice is highly ordered, and its spatial extension can exceed 1×1 mm². In order to avoid sample charging during high-resolution FE-SEM imaging and to precisely position the nanoparticle superlattices for optical measurements, copper meshes with square open apertures are covered on top of the studied nanoparticle superlattices. (b) FE-SEM image of Au@C18 HCP nanoparticle superlattice on quartz with an imaging area of 1×1.5 μm².

twice the fully extended thiolate chains. This discrepancy suggests that the alkyl chains might interdigitate with the chains on neighboring particles. Alternatively, the thiolate chains might collapse somewhat after solvent evaporation. The dependence of interparticle gap on the number of carbon atoms per chain is in agreement with previous reports.[12] However, for the case of Au@C18 superlattice, the interparticle gap increases quite abruptly from that of the Au@C16 superlattice. This phenomenon (chain-length-dependent phase transition) is consistent with the suggestion by Badia et al. that, for long-chain thiolates (>C16), the alkyl chains exist predominantly in an extended, all-*trans*-ordered conformation at room temperature, while for shorter chains, significant chain disorders exist.[13] Additional infrared spectroscopic data also support that short-chain thiolates on nanoparticles are more disordered (Figure S4). This phenomenon is probably due to the fact that the structure of 3D self-assembled monolayers (SAMs) on highly curved surfaces (nanoparticles) is different from that for 2D SAMs on planar surfaces. In the case of 2D SAMs on gold surfaces, thiolate chains are in fully extended all-*trans*-ordered conformation.

Now that we have demonstrated the self-assembly of gold nanoparticle superlattices of controlled particle size and lattice spacing, it is of paramount interest to investigate how the tunable interparticle gap can impact the CSPR properties of these tailored superlattices. Figure 3a shows the optical extinction spectra obtained from four different thiolate-stabilized nanoparticle superlattices. These spectra were obtained using a microspectroscopic measurement setup [$\sim$7 μm beam diameter (normal incident, unpolarized light), corresponding to a coverage of $\sim10^5$ nanoparticles]. Optical measurements were performed over five different regions of nanoparticle superlattices, and the displayed spectra were the
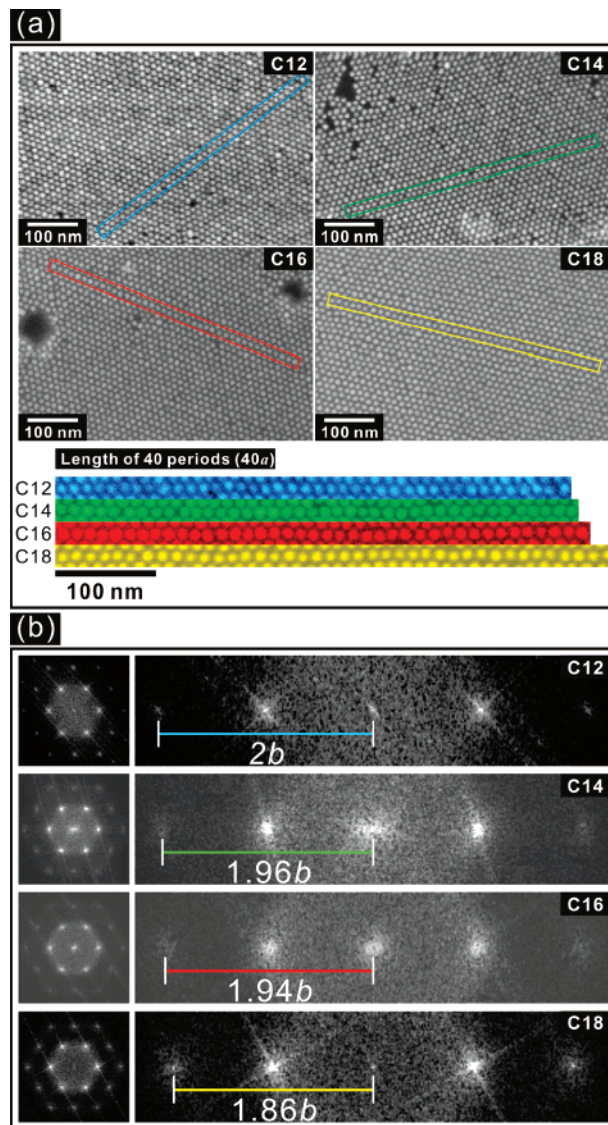

Figure 2. (a) FE-SEM images of Au@C12, Au@C14, Au@C16, and Au@C18 HCP nanoparticle superlattices on quartz substrates. In order to estimate the lattice constants (a) for nanoparticle superlattices, the lengths of 40 lattice periods (40a) are measured using FE-SEM images on five different superlattice regions and the average periods are obtained as the following: 12.80 $\pm$ 0.06 nm (Au@C12), 13.00 $\pm$ 0.15 nm (Au@C14), 13.30 $\pm$ 0.13 nm (Au@C16), and 13.90 $\pm$ 0.10 nm (Au@C18). In the bottom part of panel a, typical line-cut FE-SEM images are shown. (b) Diffraction patterns obtained from fast Fourier transform of 742 $\times$ 742 nm² (512 $\times$ 512 pixels) high-resolution FE-SEM images. From the patterns, we can determine the reciprocal-space lattice constants (from center to second order spot) and compare them with that of real-space lattice shown in panel a.

averaged results. The measured extinction peak positions are accurate within 2 nm. In Figure 3a, pronounced red shifts (32 nm for a small interparticle gap change of $\sim$1.1 nm between Au@C12 and Au@C18) in the CSPR bands can be clearly observed. Furthermore, the shift in maximum extinction wavelength exhibits an exponential dependence on the gap distance (Figure 3b) as predicted earlier by electrodynamic simulations.[9b]

The observed red shifts in the peak positions of surface plasmon resonance bands are much larger than any known wavelength shifts by varying particle size (negligible in the quasi-static regime, 3 nm < d < 25 nm)[2] or dielectric environment ($\sim$10 nm shift for change of refractive index n from 1.33 to 1.46).[3] Especially, the nanoparticles in these superlattices have the same metal core size
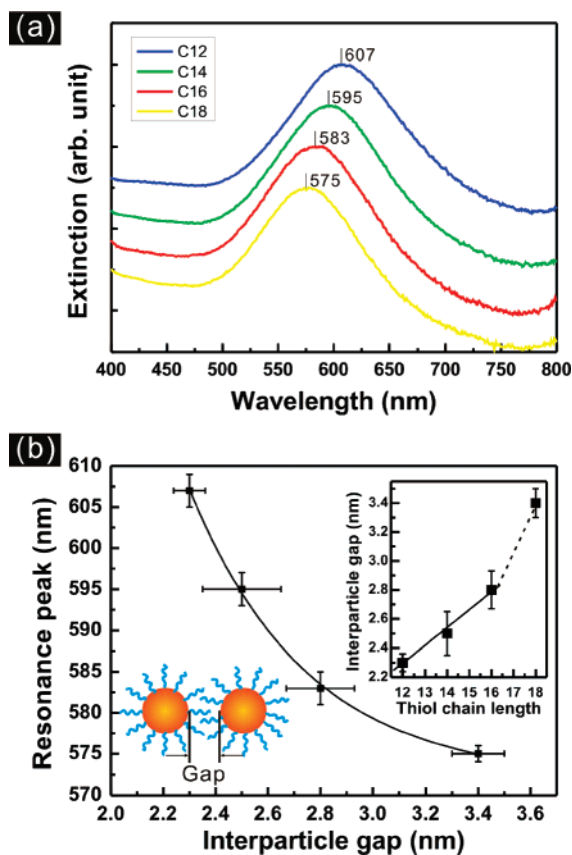
Figure 3. (a) Optical extinction spectra of four kinds of thiolate-stabilized nanoparticle superlattices with the same metal core size, but different in alkyl chain length. (b) Exponential dependence of the resonance peak position on the interparticle gap. The inset shows the relation between interparticle gap and thiolate chain length using the lattice constants obtained in Figure 2 and the known nanoparticle core size of 10.5 nm.

(~10.5 nm), and the dielectric constants of alkanethiolates are nearly constant ($n_{thiolate} \approx n_{quartz} \approx 1.46$). Therefore, the large shifts observed in the CSPR bands are indicative of strong interparticle interactions. Here, the evidence of near-field coupling for the observed CSPR bands comes from their gap-distance-dependent behavior. For the cases of arrays of large-sized and more separated (much longer than the near-field decay lengths) nanoparticles prepared by EBL, a linear blue shift for decreasing lattice spacing has been reported experimentally,[7] and it was proposed to originate from long-range dipolar interaction.[9] On the other hand, for near-field coupling, an exponentially dependent red shift for decreasing lattice spacing in nanoparticle arrays has been theoretically predicted.[9b] In previous experiments for pairs of near-field-coupled gold nanoparticles prepared by EBL,[5,14] this behavior has also been confirmed.

In a recent experiment performed by Jain et al., the measured near-field plasmonic coupling in EBL-fabricated metal nanoparticle pairs shows the universal scaling behavior of the exponential distance decay, in which the CSPR shift exponentially depends on the interparticle gap over a distance of ~20% of the metal core

size.[14] This value is within the range of the interparticle gaps observed here (Table S2) and is in agreement our interpretation of CSPR due to near-field coupling. However, the magnitude of the observed spectral shift with decreasing interparticle gap is much larger due to stronger near-field plasmonic coupling in HCP nanoparticle arrays. In contrast, for conventional nanoparticle superlattices ($d \leq 5$ nm), it would be very difficulty to observe the near-field coupling effects.

In conclusion, the approach presented here provides a unique and viable means of building bottom-up plasmonic crystals with precisely designed optical properties via near-field coupling, which cannot be easily achieved by conventional methods based on electron beam lithography.

Supporting Information Available: Experimental procedures, four figures, and two tables. This material is available free of charge via the Internet at http://pubs.acs.org.

References

(1) (a) Kreibig, U.; Vollmer, M. *Optical Properties of Metal Clusters*; Springer-Verlag: Berlin, 1995. (b) Kelly, K. L.; Coronado, E.; Zhao, L. L.; Schatz, G. C. *J. Phys. Chem. B* **2003**, *107*, 668−677.
(2) Link, S.; El-Sayed, M. A. *J. Phys. Chem. B* **1999**, *103*, 4212−4217.
(3) (a) Underwood, S.; Mulvaney, P. *Langmuir* **1994**, *10*, 3427−3430. (b) Alvarez, M. M.; Khoury, J. T.; Schaaff, T. G.; Shafigullin, M. N.; Vezmar, I.; Whetten, R. L. S. *J. Phys. Chem. B* **1997**, *101*, 3706−3712. (c) Templeton, A. C.; Pietron, J. J.; Murray, R. W.; Mulvaney, P. *J. Phys. Chem. B* **2000**, *104*, 564−570.
(4) (a) Taleb, A.; Petit, C.; Pileni, M. P. *J. Phys. Chem. B* **1998**, *102*, 2214−2220. (b) Ung, T.; Liz-Marzán, L. M.; Mulvaney, P. *J. Phys. Chem. B* **2001**, *105*, 3441−3452. (c) Malynych, S.; Chumanov, G. *J. Am. Chem. Soc.* **2003**, *125*, 2896−2898.
(5) (a) Rechberger, W.; Hohenau, A.; Leitner, A.; Krenn, J. R.; Lamprecht, B.; Aussenegg, F. R. *Opt. Commun.* **2003**, *220*, 137−141. (b) Su, K.-H.; Wei, Q.-H.; Zhang, X.; Mock, J. J.; Smith, D. R.; Schultz, S. *Nano Lett.* **2003**, *3*, 1087−1090. (c) Gunnarsson, L.; Rindzevicius, T.; Prikulis, J.; Kasemo, B.; Käll, M.; Zou, S.; Schatz, G. C. *J. Phys. Chem. B* **2005**, *109*, 1079−1087.
(6) Maier, S. A.; Kik, P. G.; Atwater, H. A.; Meltzer, S.; Harel, E.; Koel, B. E.; Requicha, A. A. G. *Nat. Mater.* **2003**, *2*, 229−232.
(7) (a) Haynes, C. L.; McFarland, A. D.; Zhao, L.; Van Duyne, R. P.; Schatz, G. C.; Gunnarsson, L.; Prikulis, J.; Kasemo, B.; Käll, M. *J. Phys. Chem. B* **2003**, *107*, 7337−7342. (b) Bouhelier, A.; Bachelot, R.; Im, J. S.; Wiederrecht, G. P.; Lerondel, G.; Kostcheev, S.; Royer, P. *J. Phys. Chem. B* **2005**, *109*, 3195−3198.
(8) (a) Barnes, W. L.; Dereux, A.; Ebbesen, T. W. *Nature* **2003**, *424*, 824−830. (b) Maier, S. A.; Atwater, H. A. *J. Appl. Phys.* **2005**, *98*, 011101. (c) Ozbay, E. *Science* **2006**, *311*, 189−193.
(9) (a) Lamprecht, B.; Schider, G.; Lechner, R. T.; Ditlbacher, H.; Krenn, J. R.; Leitner, A.; Aussenegg, F. R. *Phys. Rev. Lett.* **2000**, *84*, 4721−4724. (b) Zhao, L.; Kelly, K. L.; Schatz, G. C. *J. Phys. Chem. B* **2003**, *107*, 7343−7350.
(10) Ditlbacher, H.; Hohenau, A.; Wagner, D.; Kreibeg, U.; Rogers, M.; Hofer, F.; Aussenegg, F. R.; Krenn, J. R. *Phys. Rev. Lett.* **2005**, *95*, 257403.
(11) (a) Brust, M.; Walker, M.; Bethell, D.; Schiffrin, D. J.; Whyman, R. *J. Chem. Soc., Chem. Commun.* **1994**, 801−802. (b) Tzeng, S. D.; Lin, K. J.; Hu, J. C.; Chen, L. J.; Gwo, S. *Adv. Mater.* **2006**, *18*, 1147−1151.
(12) (a) Fink, J.; Kiely, C. J.; Bethell, D.; Schiffrin, D. J. *Chem. Mater.* **1998**, *10*, 922−926. (b) Motte, L.; Pileni, M. P. *J. Phys. Chem. B* **1998**, *102*, 4104−4109. (c) Martin, J. E.; Wilcoxon, J. P.; Odinek, J.; Provencio, P. *J. Phys. Chem. B* **2000**, *104*, 9475−9486. (d) Lin, X. M.; Jaeger, H. M.; Sorenson, C. M.; Klabunde, K. J. *J. Phys. Chem. B* **2001**, *105*, 3353−3357.
(13) (a) Badia, A.; Singh, S.; Demers, L.; Cuccia, L.; Brown, G. R.; Lennox, R. B. *Chem.−Eur. J.* **1996**, *2*, 359−363. (b) Badia, A.; Cuccia, L.; Demers, L.; Morin, F.; Lennox, R. B. *J. Am. Chem. Soc.* **1997**, *119*, 2682−2692.
(14) Jain, P. K.; Huang, W.; El-Sayed, M. A. *Nano Lett.* **2007**, *7*, 2080−2088.

JA0773610